scientific reports

Check for updates

OPEN

Fabrication of selective and sensitive chemical sensor probe based on ternary nano-formulated $CuO/MnO_2/Gd_2O_3$ spikes by hydrothermal approach

Mohammed M. Rahman[1,2]✉, M. M. Alam[3], Abdullah M. Asiri[1,2] & Firoz A. D. M. Opo[4,5]

In this approach, thin spikes (NSs) of ternary nano-formulated mixed $CuO/MnO_2/Gd_2O_3$ were synthesized by the hydrothermal approach for efficient detection of 3-methoxyphenyl hydrazine (3-MPHyd) chemical from various environmental samples. The NSs were systematically characterized by using XPS, EDS, TEM, FTIR, UV/vis, and XRD. The fabricated NSs onto the glassy carbon electrode (GCE) was successfully applied for the selective and sensitive detection of 3-MPHyd in the phosphate buffer system (PBS), which displayed the highest sensitivity, good selectivity with ultra-trace detection limit, high stability, good reproducibility, and quick response time. The real environmental samples were tested for validation from stand point of the ternary doped nanomaterials for sensing in the practical applications using by electrochemical method.

As strong reducing agents, generally the phenyl hydrazine and their derivatives are well-known, and they have various industrial applications such as blooming agent for plastics, corrosion inhibitor insecticides, and oxygen scavenger in the boiler as rocket fuel, photographic chemicals, aerospace fuel and explosives[1]. Due to exposure of these chemicals by human even at trace amount, may cause the hostile effect to human such as liver and kidney injury, haemolytic anaemia, skin irritation and dermatitis, etc. and the phenyl hydrazine and their derivatives are considered as a carcinogenic[2–4]. Then it is necessary to capture of 3-MPHyd at ultra-trace level to safe the human, environment, and the eco-system. The literatures have been described the detection methods of phenyl hydrazine and their derivatives such as fluorimetry, capillary electrophoresis, chromatography, spectrophotometry, photometry and photometric titrations, electrochemical technique[5–7]. But most of them, the electrochemical methods are widely implemented technique due to its high sensitivity, lower detection limit, greater simplicity, lower cost and long-term stability in chemical environment. Except few articles, the most of reported studies have been suffering in sensitivity, reproducibility and stability. To the phenyl hydrazine and their derivatives, the higher potential is required for GCE. Therefore, the modified GCE needs easy to fabricate for increasing the electrons transferring-rate as well as improving the sensitivity with lower detection limit[8].

To reduce the over potential and increase the electron transfer rate, the various transition material such as copper oxides are used as detecting or capturing materials to the phenyl hydrazine and their derivatives[9]. Recently, the un-doped metal oxides (specially, transition) such as iron oxide, tungsten oxide, manganese oxide, and copper oxide are also studied as a detecting material of hydrazine and the derivatives of hydrazine[10]. Among them, MnO_2 is the potential electron arbitrator as exhibited the high catalytic activity, precise surface area, lower resistances and pleasant electrochemical properties[11]. The CuO is a good electro mediator with better electro-chemical property with large surface area, which can enhance the electron transferring[12]. Generally, nanostructure materials have given significant attention for various organic as well as inorganic components, which is attracted owing to the binding affinity at optimum working conditions[13–16].

[1]Department of Chemistry, Faculty of Science, King Abdulaziz University, P.O. Box 80203, Jeddah 21589, Saudi Arabia. [2]Center of Excellence for Advanced Materials Research (CEAMR), King Abdulaziz University, P.O. Box 80203, Jeddah 21589, Saudi Arabia. [3]Department of Chemical Engineering and Polymer Science, Shahjalal University of Science and Technology, Sylhet 3100, Bangladesh. [4]Department of Biomedical Science, College of Natural Sciences, Chosun University, Chosun, South Korea. [5]Phytochemistry Research Laboratory, Department of Pharmacy, University of Asia Pacific, Dhaka, Bangladesh. ✉email: mmrahman@kau.edu.sa

A successful hydrazine derivative material with zinc oxide nano-urchins is reported and exhibited the good sensitivity as well as lower detection limit[17]. Another hydrazine derivate material based on silver-doped zinc oxide was reported, which was successful with high sensitivity and detection limit[18]. It is already established that CuO and MnO_2 are efficient sensing elements to monitor the toxins for the safety of environment. Therefore, the ternary combination of $CuO/MnO_2/Gd_2O_3$ NSs may be an effective detection material to detect environmental toxins due to the large active surface area in their interior or exterior surfaces. Various toxic analytes such as phenols and their derivatives, alcohol, acetone, ammonium hydroxide, dichloromethane, heavy-metal ions, hydrazine, aliphatic and aromatic compounds have been detected by various compositions of metal oxide/sulphides with the doped or un-doped, mixed/dual combinations[19]. The nanostructure materials prepared by sol–gel method have been shown elsewhere with the higher surface area for good adsorption of chemicals and ions[20–23]. From the specific advantage of the active surface area with ternary metal oxides compared to single or dual/doped combination, it is highly demanded to introduce new doped materials with metal oxides.

Generally, mixed doped metal oxide exhibits promising results for the detection and quantification of hazardous chemicals by various detection approaches. Besides this, as enhancing of electrochemical properties of $CuO/MnO_2/Gd_2O_3$ NS nanostructure material by converting it to a doped mixed oxides with other materials is also cost-effective. Here, $CuO/MnO_2/Gd_2O_3$ NS nanostructured materials have employed a great deal of consideration due to their chemical, structural, physical, and optical properties in terms of large-active surface area, high-stability, and high porosity. These properties are directly depend on the structural morphology prepared by reactant precursors for making the $CuO/MnO_2/Gd_2O_3$ porous materials in the basic medium at low-temperature. This $CuO/MnO_2/Gd_2O_3$ NSs material was synthesized by a facile solution method using NaOH solution. This technique has several advantages including facile preparation, accurate control of reactant temperature, easy to handle, one-step reaction. Optical, morphological, electrical, and chemical properties of the $CuO/MnO_2/Gd_2O_3$ NS nanomaterials are of huge significance from the scientific aspect, compared to other undoped materials. The non-stoichiometry, mostly oxygen vacancies, Gd_2O_3 makes it conducting nature in the doped nanostructured materials[24–29]. The formation energy of oxygen vacancies and metal interstitials in the semiconductor is very low and thus these defects form eagerly, resulting the increased conductivity of $CuO/MnO_2/Gd_2O_3$ NS materials compared to other undoped materials. $CuO/MnO_2/Gd_2O_3$ NS materials have also attracted considerable interest due to their potential applications in fabricating optoelectronic, electro-analytical, selective detection of assays, chemical sensor devices, hybrid-composites, electron-field emission sources for emission exhibits, biochemical detections, and surface-enhanced Raman properties, etc. $CuO/MnO_2/Gd_2O_3$ NS material offers improved performance due to the large-active surface area, which increased conductivity and current responses of the $CuO/MnO_2/Gd_2O_3$ NSs/Nafion/GCE assembly during the electrochemical investigation.

The most reliable hydrothermal process was applied to synthesize $CuO/MnO_2/Gd_2O_3$ NSs. The fabricated NSs were practice for the coating onto a GCE, and the binding properties between these were enhanced by the addition of nafion solution. The resulted GCE was investigated for efficient capturing of 3-MPHyd in the aqueous media. The analytical capturing performances were studies very carefully, and the outcome of the 3-MPHyd chemical material was high sensitivity with the low detection limits. Here, it is introduced a significant material in this approach for selective and sensitive monitoring and capturing of selective 3-MPHyd with $CuO/MnO_2/Gd_2O_3$ NSs sensor probe.

Experimental section

Materials and method. In this research work, the required chemicals were used as received without further purification. The inorganic salts of transition metals such as copper(II) chloride ($CuCl_2$), manganese(II) chloride ($MnCl_2$), gadolinium(III) chloride, and ammonium hydroxide (NH_4OH) were purchased from well-known Sigma-Aldrich, which was deployed to prepare ternary $CuO/MnO_2/Gd_2O_3$ NSs. As a part of these studies, the analytical grade chemicals 2,4-DNP (2,4-dinitrophenol), 3,4-DAT (3,4-diaminotoluene), pyridine, BH (benzaldehyde), 3-chlorophenol, THF (tetrahydrofuran), methanol, 3-MPHyd (3-methoxyphenylhydrazine), AH (ammonium-hydroxide), coating agent nafion (in 5% ethanol), NaH_2PO_4, and Na_2HPO_4 were also bought from the Sigma-Aldrich and deployed as-received. For the details characterization of synthesized $CuO/MnO_2/Gd_2O_3$ NSs, conventional XRD, XPS, FTIR, UV/Vis and FESEM were implemented to evaluate the structural, crystalline, functional, optical, morphological and elemental analyses. The reliable current versus potential (electrochemical method) was used to determine 3-MPHyd with active $CuO/MnO_2/Gd_2O_3$ NSs material by using Keithley electrometer (6517A, USA) at room conditions.

Hydrothermally synthesis of $CuO/MnO_2/Gd_2O_3$ NSs. The inorganic salts copper chloride ($CuCl_2$), manganese chloride ($MnCl_2$), gadolinium chloride ($GdCl_3$) and alkali ammonium hydroxide (NH_4OH) were used to prepare $CuO/MnO_2/Gd_2O_3$ NSs by solvo/hydrothermal method at low temperature. The solvothermal process was widely used efficient method to fabricate nanomaterials of metal oxides, and the resultant guest or doped metal oxides are smaller in size as well as phase formation. Following this method, 100.0 mL of 0.10 M $CuCl_2$, 100.0 mL of 0.10 M $MnCl_2$, 100.0 mL of 0.10 M $GdCl_3$ and 100.0 mL of 0.10 M NH_4OH were prepared in a different four 200.0 mL beaker with de-ionized water and resultant solutions were kept with continuous magnetic stirring. Another 250.0 mL of conical flask was taken and 50.0 mL of each prepared metallic salt solution was added. Then the mixture was shacked with continuous magnetic stirring onto the hot plate. To obtain the co-precipitation of metal hydroxides, the prepared 0.10 M NH_4OH was added slowly and at the pH value 10.5, all metal hydroxides were precipitated out in conical flask. Then the total solution was kept at 80 °C on the hot plate with continuous magnetic stirring around 6 h. As-prepared participate of metal hydroxides were washed thoroughly by de-ionized water and kept it to dry at room condition for overnight. Consequently, the powdered sample was heated for calcination at 510 °C for 6 h. Under higher temperature, the metal oxides is transform to

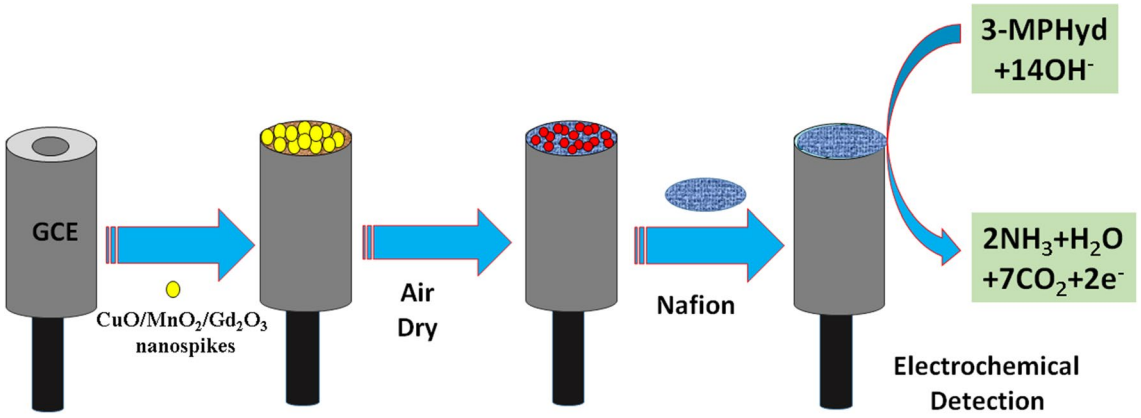

Figure 1. Fabrication of GCE with ternary doped $CuO/MnO_2/Gd_2O_3$ NSs by using 5% nafion conducting coating binder.

crystalline metal oxide i.e., $CuO/MnO_2/Gd_2O_3$ nanostructure shapes, which contains the higher metallic-ions. The prepared material was properly grained into fine powder of nano-sized materials for details characterization. The following reactions may happen:

In the aqueous medium:

$$NH_4OH_{(s)} \rightarrow NH^+_{4(aq)} + OH^-_{(aq)} \quad (1)$$

$$CuCl_{2(s)} \rightarrow Cu^{2+}_{(aq)} + 2Cl^-_{(aq)} \quad (2)$$

$$MnCl_{2\,(s)} \rightarrow Mn^{2+}_{(aq)} + 2Cl^-_{(aq)} \quad (3)$$

$$GdCl_{3(s)} \rightarrow Gd^{3+}_{(aq)} + 3Cl^-_{(aq)} \quad (4)$$

$$NH^+_{4(aq)} + 7OH^-_{(aq)} + Cu^{2+}_{(aq)} + Mn^{2+}_{(aq)} + Gd^{3+}_{(aq)} + Cl^-_{(aq)} \rightarrow Cu(OH)_2/Mn(OH)_2/Gd(OH)_{3(aq)} \downarrow + NH_4Cl_{(aq)}. \quad (5)$$

In furnace:

$$Cu(OH)_2/Mn(OH)_2/2Gd(OH)_{3(aq)} + {}^1/_2\,O_2 \rightarrow CuO/MnO_2/Gd_2O_{3(s)} + 5H_2O \uparrow . \quad (6)$$

The *Ks* was low ($Ks = 2.2 \times 10^{-20}$ in $Cu(OH)_2$, 2.0×10^{-13} for $Mn(OH)_2$ and 1.88×10^{-23} for $Gd(OH)_3$[30]. Metal ions were precipitated out quantitatively as various oxides. The crystal formation was happened initially, where an aggregation to the $Gd(OH)_3$ was started. In the reaction system, pH was continued to enhance, then the $Cu(OH)_2$ was started to precipitate, which was re-aggregated onto the $Gd(OH)_3$ crystallites. Further increasing of pH, $Mn(OH)_2$ is also participated out to form aggregation with other two metal hydroxides. The formation of NSs is similar with the previously reported article[31]. The synthesized NSs were characterized in terms of elemental composition, crystallinity, optical property, morphology, structure, and functional properties. Later, $CuO/MnO_2/Gd_2O_3$ NSs were applied to detect 3-MPHyd by reliable electrochemical method at room conditions. This is the first time, the produced $CuO/MnO_2/Gd_2O_3$ NSs were implemented for the selective determination of 3-MPHyd for environmental safety by electrochemical method.

Fabrication of $CuO/MnO_2/Gd_2O_3$/Nafion/GCE sensor probe. The ternary doped materials based on the NSs of $CuO/MnO_2/Gd_2O_3$ was successively implemented to determine the target environmentally unsafe 3-MPHyd in reaction medium. To prepare the working electrode for 3-MPHyd detection, the ethanolic slurry of $CuO/MnO_2/Gd_2O_3$ NSs was put onto the GCE. Platinum wire (Pt-wire) was used as a counter electrode. The dispersed materials was attached between NSs of ternary metal oxides and GCE by air dry initially. It was fabricated on the flat GCE and dried in air for complete thin-film formation. Later, after drying completely, 1.0 µL of 5.0% Nafion (ethanolic) was dropped onto the fabricated electrode surface and waited until dry it completely. Here, nafion is used as a chemical glue for the stable attachment of ternary materials onto the surface of flat-GCE. Then the dried fabricated electrode was used as working electrode in this investigation. The electrochemical cell was composed by $CuO/MnO_2/Gd_2O_3$/binders/GCE sensor probe as working electrode. The fabrication scheme is presented in the Fig. 1. The target analyte 3-MPHyd was used to prepare the solution in di-ionized water on the concentration range from 1.0 mM to 1.0 pM and this formulated solutions of 3-MPHyd (lower to higher concentration) were investigated into electrochemical cell (chemical material). Then the linear-

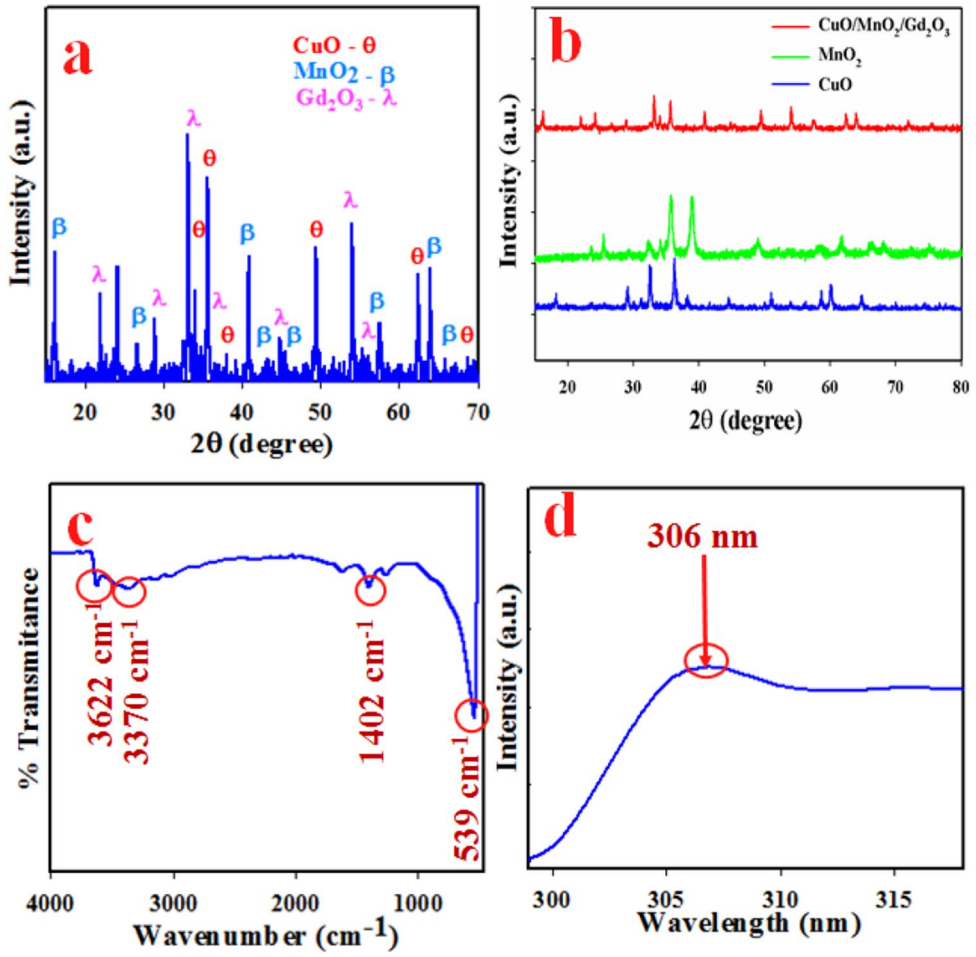

Figure 2. Structural and optical characterization of ternary doped $CuO/MnO_2/Gd_2O_3$ NS materials. (**a**) XRD pattern of $CuO/MnO_2/Gd_2O_3$ NSs, (**b**) XRD of CuO, MnO_2, Gd_2O_3 NSs, (**c**) FTIR of $CuO/MnO_2/Gd_2O_3$ NSs, and (**d**) UV absorbance of the $CuO/MnO_2/Gd_2O_3$ NSs.

ity was calculated from the linear plot by using regression co-efficient (r^2). The other analytical properties of 3-MPHyd chemical sensor such as LDR and LOD were estimated according to ratio of 3 N/S.

Results and discussion

Materials properties. The crystallographic studies of prepared $CuO/MnO_2/Gd_2O_3$ NSs were carried out by the implementation of XRD. As shown in Fig. 2a, the fabricated NSs were consisting of diversified crystalline mediums of CuO, MnO_2 and Gd_2O_3. The resultant XRD spectra is represented the Bragg planes of CuO indices as θ such as (110), (111), (200), (202), (113), and (022), which has the similarities with JCPDS No. 72-0629 and earlier published articles[32,33]. The other diffracted peaks created from MnO_2 indices as ß are (101), (110), (111), (200), (210), (211), (002) and (310). This XRD pattern of MnO_2 is agreed with the JCPDS Card, No. 24-0735 and literatures[34,35]. The additional sharpest peaks of Gd_2O_3 indices as λ are (211), (222), (411), (442), (611) and (622), which are agreed with those reported for gadolinium oxide nanoparticles[36] and JCPDS No. 43-1015. There is a provision for measuring the crystallinity by the XRD pattern through Scherer's expectation (vii).

$$D = 0.9\lambda/(\beta \cos\theta) \tag{7}$$

where λ is wavelength (1.5418 Å) and β is width at half, according to the apex peak, and θ is the diffracting edge[37]. Here, the determined crystallinity was 43.31 nm. Additionally, it is also compared the XRD spectrum of individual CuO, MnO_2, and $CuO/MnO_2/Gd_2O_3$ NSs and presented in the Fig. 2b. FTIR investigation of synthesized $CuO/MnO_2/Gd_2O_3$ NSs is depicted in Fig. 2c and obtained peaks are at 539, 1402, 3370 and 3622 cm^{-1}. The main characteristic absorption peak is at 539 cm^{-1} which is corresponding to Mn–O or Cu–O stretching modes[38] and the identical peak at 1402 cm^{-1} is responsible for C–O stretching[39]. The other two peaks at 3370 and 3622 are corresponding to the OH group[40]. The visual spectra of $CuO/MnO_2/Gd_2O_3$ NSs were completed at the range between 200.0 and 800.0 nm wavelengths. As judged from Fig. 2d, the maximum intensity was inspected

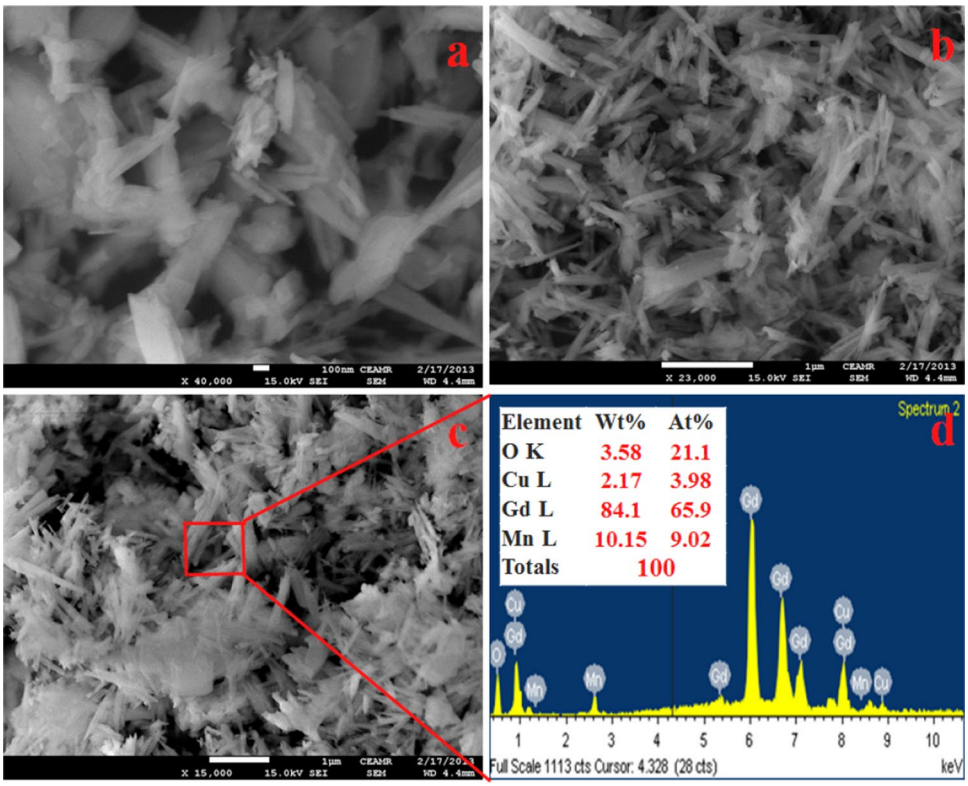

Figure 3. FESEM analysis with different morphologies (**a**,**b**) and elemental quantification of hydrothermally prepared $CuO/MnO_2/Gd_2O_3$ NSs (**c**,**d**).

at 306 nm and this was the evaluated absorption band of prepared $CuO/MnO_2/Gd_2O_3$ NSs[41]. According to the Eq. (8), the defined energy band-gap (E_{bg}) was 4.05 eV of the $CuO/MnO_2/Gd_2O_3$ NSs.

$$E_{bg}(\text{eV}) = \frac{1240}{\lambda}$$

where E_{bg} = energy band-gap and λ = maxima absorbed area.

Structural analyses. The structural analyses of the fabricated NSs were evaluated by FESEM images. The resultant FESEM of $CuO/MnO_2/Gd_2O_3$ NSs from higher to lower magnifying images are depicted in Fig. 3a,b and it is clearly shown a uniform aligned of $CuO/MnO_2/Gd_2O_3$ nanospikes. From Fig. 3c,d, the EDS define of $CuO/MnO_2/Gd_2O_3$ demonstrated the existence of Cu, Mn, Gd and O and the elemental arrangements of calcined co-doped metal oxides are nanospikes in shape. The atomic compositions (wt%) of $CuO/MnO_2/Gd_2O_3$ NSs are as O 3.58%, Cu 2.17%, Gd 84.1% and Mn 10.15%. Any additional peaks are not detected, which is associated with impurities. Therefore, the synthesized NSs are consisted only Cu, Mn, Gd and O.

Binding energy analysis. The XPS is defined in Fig. 4 are also investigated to evaluate the chemical composition, electronic and valance states of prepared $CuO/MnO_2/Gd_2O_3$ NSs. As it is shown the full spectrum (Fig. 4a), Cu2*p*, Mn2*p* Gd3*d* and O1*s* core level of spin orbitals are investigated. The observed O1*s* peak at 530.0 eV, which was presented in Fig. 4b and assigned to the O^{2-}[42,43]. The Cu2*p* spin orbital ruptures into $Cu2p_{3/2}$ and $Cu2p_{1/2}$ as depicted in Fig. 4c. Here, it displays the high resolution spectrum of Cu 2*p*, separated into Cu $2p_{3/2}$ and Cu $2p_{1/2}$ at 930.5 eV and 952.1 eV, respectively (Fig. c1 and c2). The distance between these Cu 2*p* main peaks positions is 21.6 eV, which agrees well with previous reports about CuO spectrum. It is also denoted to the existence of Cu^{2+} chemical state as an indication of the formation of CuO, which is matched to the reported literatures[44–52]. Moreover, additional confirmation of CuO state was seen with the broad satellite peaks at a higher binding energy than the main peaks. The main peak of Cu $2p_{3/2}$ at 930.5 eV was accompanied by satellite peaks on the higher binding energy side at 939.2 eV, 941.5 eV and 943.1 eV, which suggests the existence of CuO. From the full spectrum, we can clearly see that the main peak of Cu $2p_{1/2}$ at 952.1 eV, which also confirms the presence of CuO. The XPS spectrum is also exhibited the two major peaks of Mn2*p* orbital and the resultant spectrum of Mn2*p* is represented in Fig. 4d. As evaluated, the spin energy of $Mn2p_{3/2}$ (641.2 eV) and $Mn2p_{1/2}$ (653.1 eV) are also the adjacent position with the reported data for MnO_2[45,46], which is presented separately in Fig. 4d1,d2. In Gd3*d* spectra (Fig. 4e), two peaks are found, where the binding-energy of strong peak at ~ 1186.0 eV is respon-

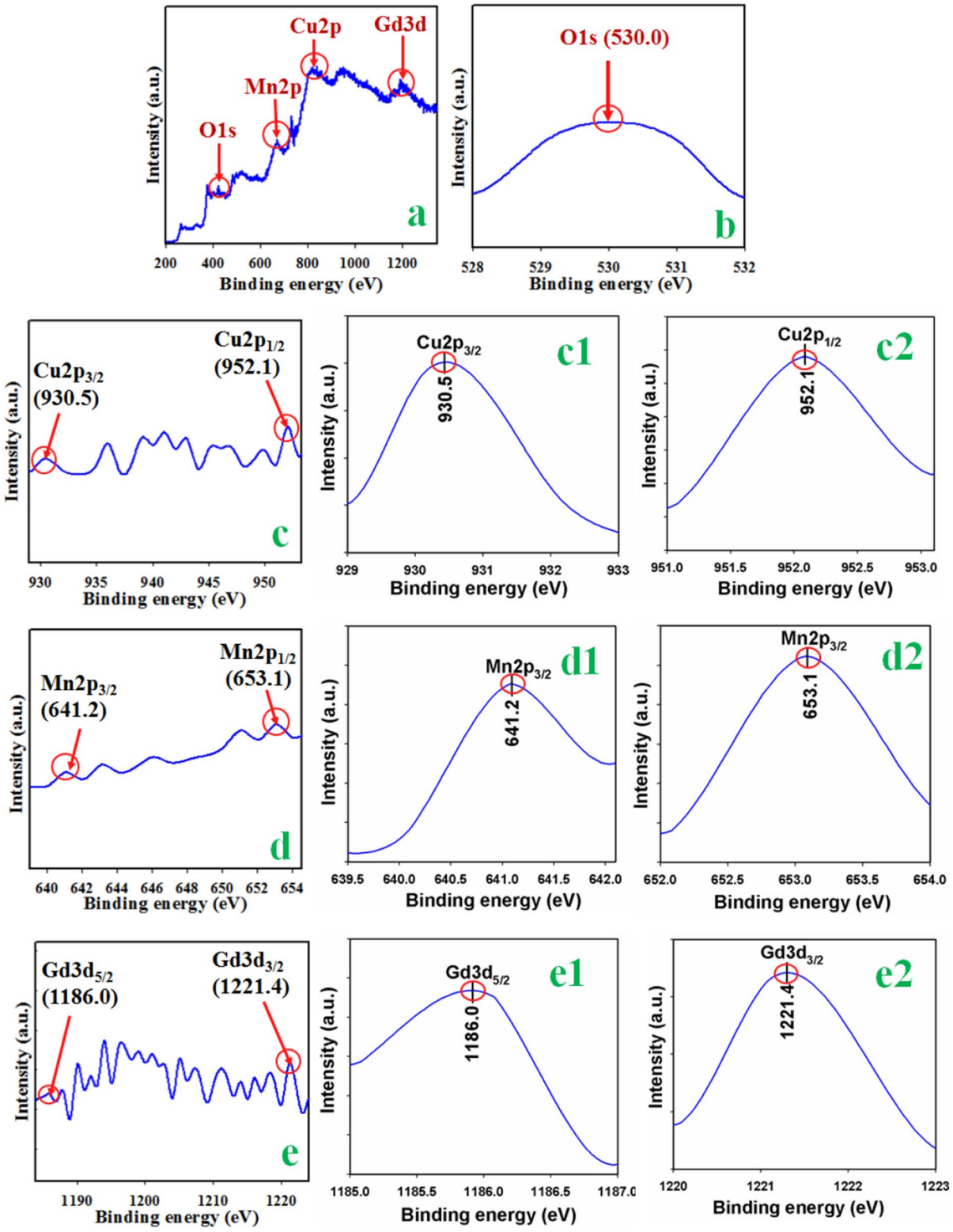

Figure 4. XPS study of doped CuO/MnO_2/Gd_2O_3 NSs. (**a**) XPS spectrum, (**b**) O1*s* level, (**c**) spin–orbit Cu2*p* level, (**c1**,**c2**) magnified peak of Cu2*p* level, (**d**) spin–orbit of Mn2*p* level, (**d1**,**d2**) magnified peak of Mn2*p* level, (**e**) spin–orbit of Gd3*d* level, and (**e1**,**e2**) magnified peaks of Gd3*d* level.

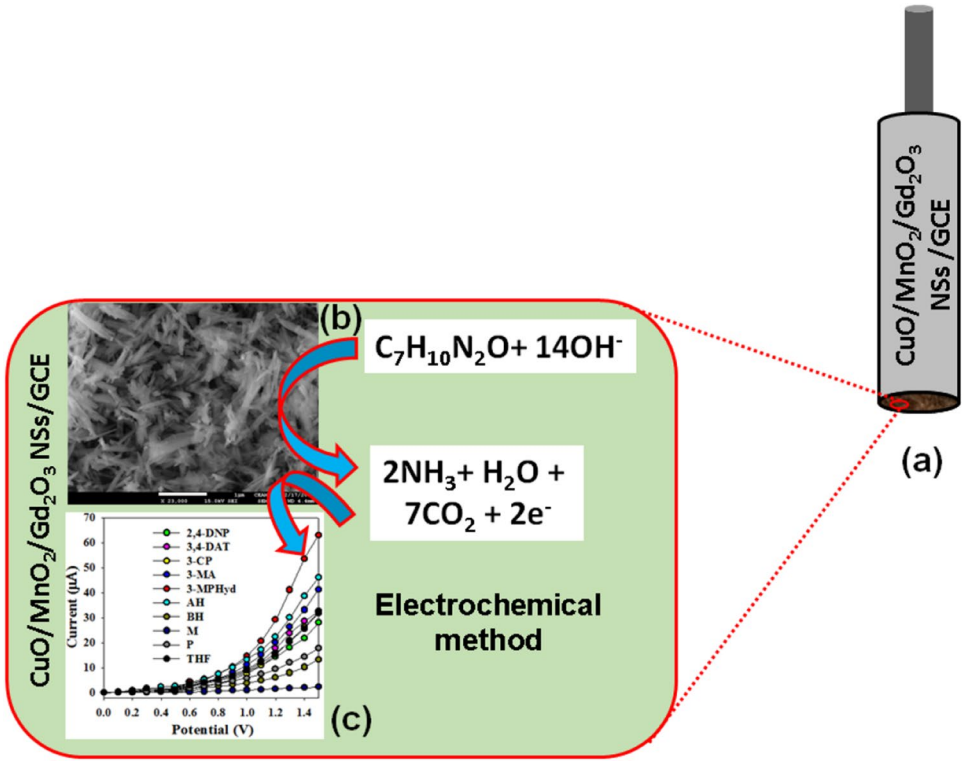

Figure 5. Schematic diagram of sensor fabrication and probable mechanism. Possible bonding mechanism of 3-MPHyd by capturing of the thin nanospikes in electrochemical approach. (**a**) GCE fabrication with CuO/MnO_2/Gd_2O_3 NSs and conducting nafion-coating binders; (**b**) Possible mechanism of 3-MPHyd capturing onto CuO/MnO_2/Gd_2O_3 NSs surfaces; (**c**) 3-MPHyd detection by electrochemical method using CuO/MnO_2/Gd_2O_3 NSs modified GCE.

sible for Gd3$d_{5/2}$, and the binding-energy of weak peak at ~ 1221.4 eV is responsible for Gd3$d_{3/2}$. It is associated with the oxidation state of Gd^{3+}, which is represented in the Fig. 4e1, e2[49,50].

Sensing of 3-MPHyrd by CuO/MnO₂/Gd₂O₃ NSs. The proposed application of 3-MPHyrd chemical material was to detect 3-MPHyrd in environmental real samples. The chemical material based on CuO/MnO_2/Gd_2O_3 NSs is first stage, and any report regarding phenyl hydrazine analyte is not available. Here the conducting binder of nafion is used to enhance the stability with high conductivity and electron transfer[51,52]. During the sensing performances of proposed 3-MPHyd chemical material, electrochemical responses of CuO/MnO_2/Gd_2O_3 NSs were increased with increasing of 3-MPHyd amount. In presence of higher concentration of target analyte, the resultant current is gradually increased by oxidation of 3-MPHyd onto CuO/MnO_2/Gd_2O_3 NSs. In this investigation, the flat GCE was coated with the ethanolic slurry of CuO/MnO_2/Gd_2O_3 NSs and dried it in the ambient temperature. Later, the fabricated CuO/MnO_2/Gd_2O_3 NSs/Nafion/GCE electrode was employed to sensing the 3-MPHyd by electrochemical approach at room conditions. The 3-MPHyd sensing mechanism onto CuO/MnO_2/Gd_2O_3 NS probe is based on the ternary metal oxides, owing to adsorption/absorption of aqueous oxygen onto the exterior or interior surface of CuO/MnO_2/Gd_2O_3 NSs, according to the dissolved O_2 in bulk-solution or surface-air of the surrounding atmosphere (Eqs. 9–11). These reactions are taken place in bulk-solution or air/liquid interface or surrounding air due to the low carrier concentration, which probably increased the resistance of ternary material surface as well as decreased the conductivity[53–56]. The anlayte 3-MPHyd sensitivity towards CuO/MnO_2/Gd_2O_3 NSs could be attributed to the high oxygen deficiency and defect the density leads to increase the oxygen adsorption for form active as O_2^-, then O^- and finally OH^-. Larger the amount of oxygen adsorbed on the mixed CuO/MnO_2/Gd_2O_3 NSs surface, larger would be the oxidizing capability and faster would be the oxidation of 3-MPHyd.

$$e^- (\text{onto CuO/MnO}_2/\text{Gd}_2\text{O}_3 \text{ NSs surface}) + O_2 \rightarrow O_2^- \quad (9)$$

$$e^- (\text{onto CuO/MnO}_2/\text{Gd}_2\text{O}_3 \text{ NSs surface}) + O_2^- \rightarrow 2O^- \quad (10)$$

$$O^- (\text{onto CuO/MnO}_2/\text{Gd}_2\text{O}_3 \text{ NSs surface}) + H_2O \rightarrow 2OH^-. \quad (11)$$

The pictographic representation (Fig. 5a) and mechanism (Fig. 5b) of the CuO/MnO_2/Gd_2O_3 NSs modified electrode of 3-MPhyd chemical material is depicted in Fig. 5. As clarified in Fig. 5c, the electrochemical signalling

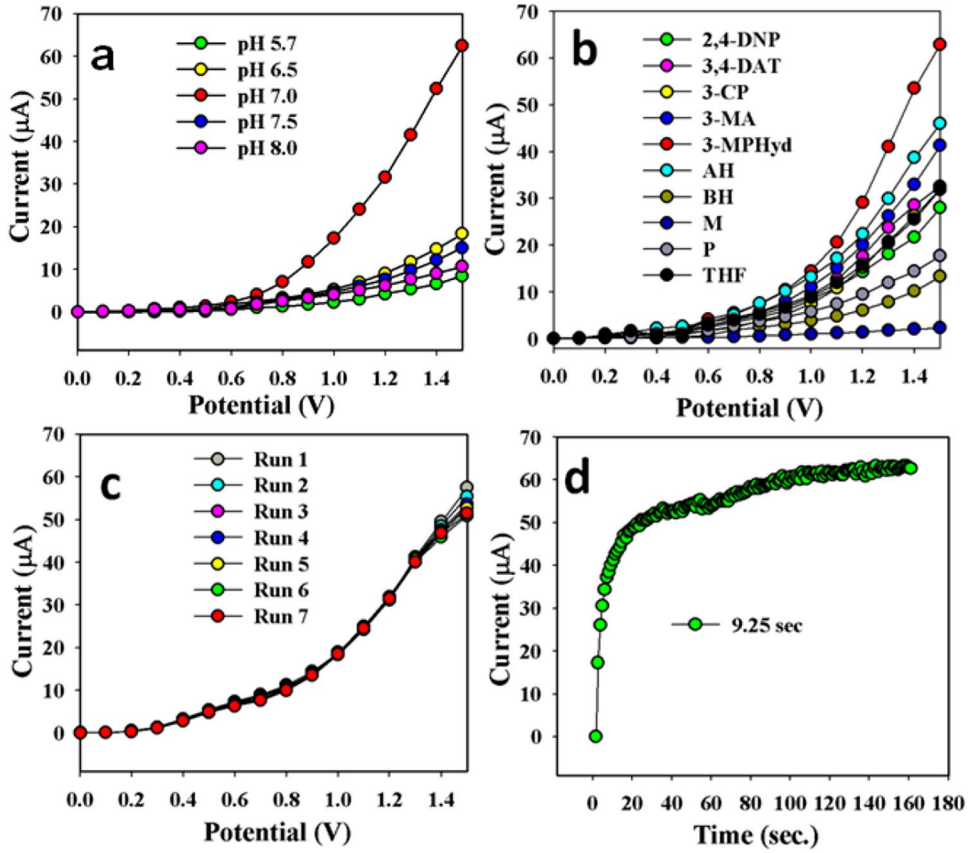

Figure 6. Optimization of 3-MPHyd chemical material based on $CuO/MnO_2/Gd_2O_3$ NSs/binder/GCE. (**a**) pH conditioning, (**b**) selectivity, (**c**) repeatability, and (**d**) response time. Analyte concentration: 0.10 nM; Holding time: 1.0 s; Electrochemical method; Potential ranges: 0 to + 1.5 V.

data was illustrated with prepared NS of $CuO/MnO_2/Gd_2O_3$, which is exhibited the higher current response compared to pure CuO and MnO_2. Here, the oxidation reaction of 3-MPHyd onto surface of $CuO/MnO_2/Gd_2O_3$ NSs/Nafion/GCE into the buffer system is proposed and presented below according to Eq. (12). According to the electrochemical oxidation process, targeted 3-MPHyd molecule is oxidized, hence released the electrons. Thus it is increased the electrochemical response with the $CuO/MnO_2/Gd_2O_3$ NSs/Nafion/GCE sensor probe in the electrochemical system during measurement of resultant current. As a result, in contact with the $CuO/MnO_2/Gd_2O_3$ NS surface, the target analyte 3-MPHyd is directly oxidized by releasing two electrons onto the sensor surface of $CuO/MnO_2/Gd_2O_3$ NSs/Nafion/GCE probe, which is measured during the electrochemical measurement at room conditions. During the oxidation of 3-MPHyd, the resultant current is significantly increased by producing ammonia, water, and carbon dioxide into the electrochemical process.

$$C_7H_{10}N_2O\ (\text{3-MPHyd}) + 14OH^-\ (\text{onto}\ CuO/MnO_2/Gd_2O_3\ \text{NS surface}) \rightarrow\ NH_3 + H_2O + 7CO_2 + 2e^- \quad (12)$$

The synthesized $CuO/MnO_2/Gd_2O_3$ NSs/binder/GCE is not equally given electrochemical response in the full range in buffer system. The invented working electrode was investigated in alkaline and acidic media, and it was observed that the chemical material was exhibited the maximum electrochemical response in pH 7.0. The pH optimization performance is illustrated in Fig. 6a. To obtain the selectivity, the fabricated working electrode based on $CuO/MnO_2/Gd_2O_3$/binder/GCE was performed in presence of various toxins such as 2,4-DNP (2,4-dinitrophenol), 3,4-DAT, pyridine, BH, 3-CP, THF, methanol, 3-MPHyd, and AH. As it is depicted in Fig. 6b, 3-MPHyd was displayed with the highest electrochemical responses. Also the most important analytical characteristic of chemical material is the ability to reproducible performance repeatedly. This performance of sensor was executed in 0.1 nM concentration of 3-MPHyd solution. The outstanding reproducibility was observed, which is shown in Fig. 6c.

The calculated RSD (relative standard deviation) is 1.10%, which is measured at + 1.0 V. The response time with the fabricated working electrode based on $CuO/MnO_2/Gd_2O_3$/binder/GCE is 9.25 s. It was evaluated under the certain amount of 0.1 nM of 3-MPHyd solution, which is shown in Fig. 6d. The fabricated sensor is very fast response towards the target analyte with $CuO/MnO_2/Gd_2O_3$/binder/GCE sensor probe by electrochemical method. After the 9.25 s, signal become sensor response become stable and flat, due to the saturation of contact surface with target analyte. The fabricated materials $CuO/MnO_2/Gd_2O_3$/binder/GCE was studied and

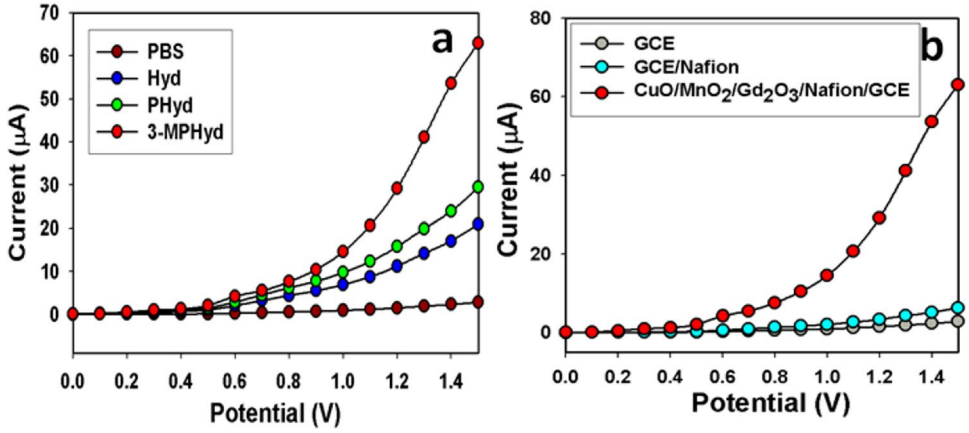

Figure 7. Control experiment of fabricated chemical sensor probe. (**a**) Comparative study of different derivatives of hydrazine such as hydrazine, phenylhydrazine, 3-methoxyphenlyhydrazines. (**b**) Comparative study of various fabricated GCE, GCE/Naifon, $CuO/MnO_2/Gd_2O_3$/Nafion/GCE electrodes. Analyte concentration: 0.1 nM; Holding time: 1.0 s; Electrochemical method; Potential ranges: 0 to + 1.5 V.

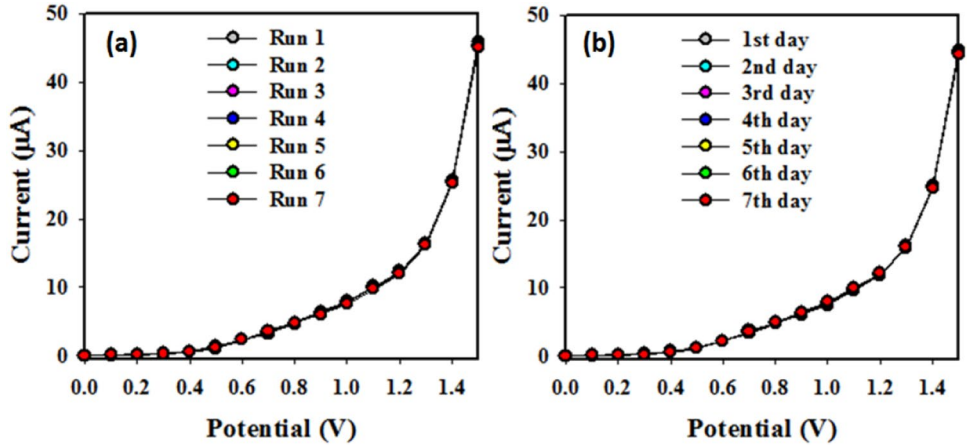

Figure 8. Optimization of $CuO/MnO_2/Gd_2O_3$/binder/GCE sensor probe. (**a**) Reproducibility study and (**b**) Inter-day validity.

compared in presence of various hydrazine derivatives (Fig. 7a). It was found that 3-MPHyd shows the highest electrochemical response (Fig. 7a) compared to blank solution (without 3-MPHyd), only hydrazine and phenylhydrazine derivatives in the identical conditions. Additionally, a control experiment has been performed with the only GCE, GCE/Nafion, and GCE/Nafion/$CuO/MnO_2/Gd_2O_3$ electrodes in the identical conditions in presence of target 3-MPHyd chemical, which is presented in the Fig. 7b. It is observed that the $CuO/MnO_2/Gd_2O_3$ fabricated glassy carbon electrode is showed the highest electrochemical current compared to only GCE and GCE/Nafion electrodes.

The materials fabricated $CuO/MnO_2/Gd_2O_3$/binder/GCE sensor probe intra-day reproducibility (Fig. 8a) and inter-day validity (Fig. 8b) have been also studied and presented in Fig. 8. According to these studies, the sensor probe is reproduced almost the similar response in the same day in different measurements in the identical conditions. On the other hand, fabricated $CuO/MnO_2/Gd_2O_3$/binder/GCE sensor probe is exhibited the almost similar reproducible responses in different inter-day measurement in the identical conditions, which is presented in the Fig. 8b.

As indicated in Fig. 9a, the electrochemical response of $CuO/MnO_2/Gd_2O_3$ NSs/binder/GCE electrode is the maximum at the lowest concentration of 3-MPHyd. To execute this performance, a range of 3-MPHyd solution was prepared based on the concentration (full range 1.0 mM to 1.0 pM) and electrochemical measurement was carried out in the range from 0.0 to + 1.5 V. The linearity (r^2: 0.9919) of the calibration plot (Fig. 9b,c was drawn as current versus concentration of 3-MPHyd). The analytical parameters have been calculated from the calibration plot (Fig. 9b) such as sensitivity (24.05 μA μM^{-1} cm^{-2}), LOD (0.4 ± 0.02 pM at SNR of 3), LDR (1.0 pM to 0.1 mM), and Response time (9.25 s). Sensitivity was calculated from the slope of the calibration plot. It was calculated from the slope of the calibration plot by considering the active surface area of fabricated electrode (0.0316 cm^2). During the sensing performances of 3-MPHyd chemical, the electrochemical current responses

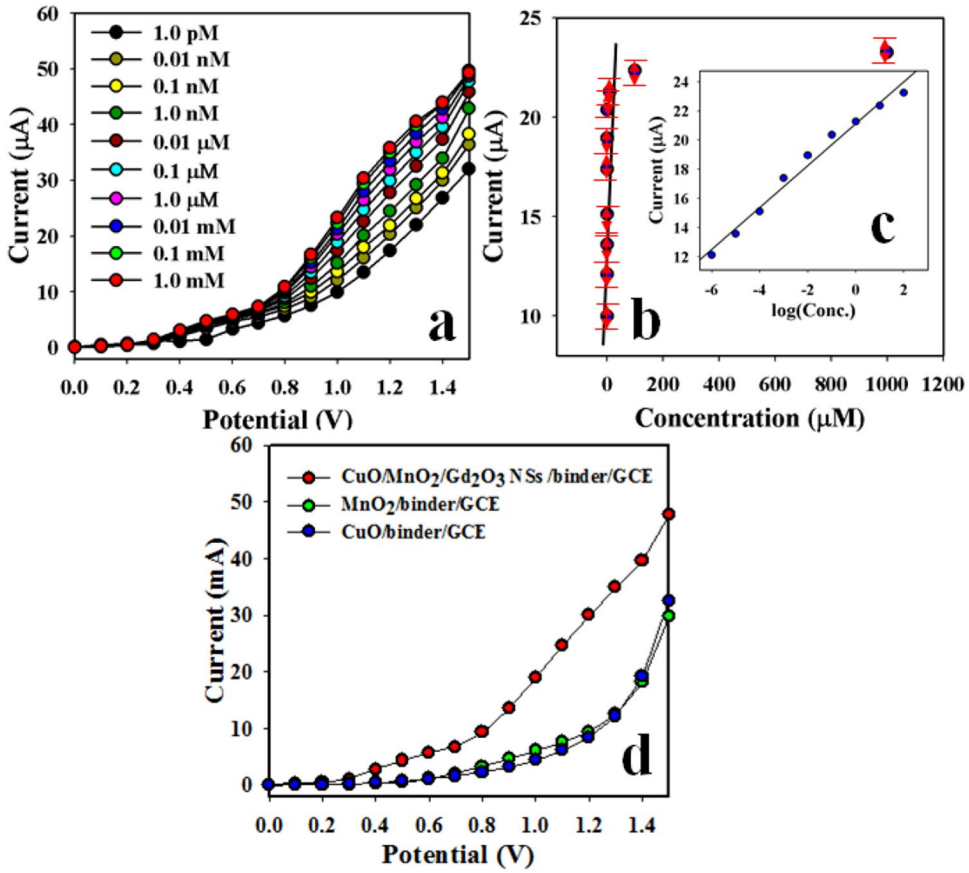

Figure 9. Detection of target chemical with the fabricated sensor probe. (**a**) Effect of concentration of 3-MPHyd compound based on $CuO/MnO_2/Gd_2O_3$ NSs by electrochemical method, (**b**) calibration curve (Inset: log [3-MPHyd. Conc.] vs. Current), and (**d**) the comparison of electrochemical responses based on various electrodes. Analyte concentration: 0.1 nM; Holding time: 1.0 s; electrochemical method; Potential ranges: 0 to + 1.5.

with $CuO/MnO_2/Gd_2O_3$ NSs were increased with increasing of the target 3-MPHyd concentration. In presence of higher concentration of target analyte, the resultant current is gradually increased due to the oxidation of 3-MPHyd during electrochemical process with $CuO/MnO_2/Gd_2O_3$ NSs. During the addition of analyte into the electrochemical solution, the oxidation current is increased gradually until 0.1 nM. After that the current response is found stable until 1.0 pM. No significant increase of current is occurred. A comparison between the electrodes fabricated on binary MnO/CuO, and ternary combinations of $CuO/MnO_2/Gd_2O_3$ NSs were studied, and it was found that $CuO/MnO_2/Gd_2O_3$ NSs/binder/GCE electrode was exhibited the highest electrochemical responses (Fig. 9d).

The possible reaction mechanism of the capturing under optimum condition is depicted in Fig. 5. The metal oxides nanomaterials are investigated as potential materials with various electroanalytical methods[57–59]. The significant application of $CuO/MnO_2/Gd_2O_3$ NSs materials was employed in the capturing of environmentally toxic compound. The $CuO/MnO_2/Gd_2O_3$ NSs materials are nontoxic, long-term stability, consistence, high electrochemical activity, nontoxicity and easy-to-use. The electrochemical method for the $CuO/MnO_2/Gd_2O_3$ NSs is considerably changed during the adsorption of 3-MPHyd as the target agent. Here, Table 1, it is presented about the materials for capturing of hydrazine and their derivatives by various electrochemical approaches[60–72]. In this nano-formulated ternary $CuO/MnO_2/Gd_2O_3$ NS materials have accomplished great deal of attention owing to their structural, chemical, optical, electrochemical, and morphological properties in terms of large-active surface area, high-stability as well as good porosity, and permeability[73–78]. This method has numerous benefits including easy and facile preparation, accurate control of the reactants temperature, easy to handle, one-step reaction, and high-porosity as well as porous natures[79–82]. Finally, this mixed $CuO/MnO_2/Gd_2O_3$ NSs material have also attracted substantial attention owing to their impending applications in fabricating chemical devices, opto-electronics, electro-analytical, selective detection of chemical and biochemical assays, hybrid-composites, electron-field emission sources for emission exhibits, and biochemical detections etc.

Real sample analysis. The ternary $CuO/MnO_2/Gd_2O_3$ NS materials fabricated electrode probe is potentiality depended on the real sample treating and others feasibility parameters[62–65]. To measure the 3-MPHyd in

Capturing layer	Analyte	Methods	Performances	References
TiO_2/CNT	Hyd	Amperometric	Sensitivity: 0.001497 μA cm^{-2} $μM^{-1}$	60
			DL: 0.22 μM	
			LDR: 0.35–162 μM	
			Linearity, $r^2 = 0.993$	
Ag/ZIF-8	Hyd	Amperometric	Sensitivity: 0.05446 μA cm^{-2} $μM^{-1}$	61
			DL: 1.57 μM (at SNR of 3)	
			LDR: 6–5000 μM	
			Linearity, $r^2 = 0.998$	
CNT powder microelectrode	Hyd	CV	Sensitivity: 0.9944 μA $μM^{-1}$ cm^{-2}	62
Ag-ZnO Nanoellipsoids	Hyd	CV	Sensitivity: 0.0946 mA $μM^{-1}$ cm^{-2}	63
			DL: 0.07 nM	
			LDR: 0.07–1.0 μM	
MWCNT and chlorogenic acid	Hyd	CV	Sensitivity: 0.0041 μA $μM^{-1}$ cm^{-2}	64
			DL: 8.0 nM	
Hierarchical micro/nanoarchitectures of ZnO	Hyd	CV	Sensitivity: 0.51 μA $μM^{-1}$ cm^{-2}	65
			DL: 0.25 nM	
			LDR: 0.8–200 μM	
Pristine ZnO NRs array	Hyd	CV	Sensitivity: 0.0448 mA $μM^{-1}$ cm^{-2}	66
			DL: 0.2 nM	
ZnO-II/Au	Hyd	CV	Sensitivity: 1.6 μA $μM^{-1}$ cm^{-2}	67
			DL: 0.066 nM	
			LDR: 0.066–425 μM	
ZnO/SWCNT	Hyd	CV	Sensitivity: 0.1 μA$μM^{-1}$ cm^{-2}	68
			DL: 0.17 nM	
			LDR: 0.5–50 μM	
ZnO Nanoflowers	Hyd	CV	Sensitivity: 0.0349 mA $μM^{-1}$ cm^{-2}	69
			DL: 0.18 nM	
Nano-Au ZnO-MWCNT	Hyd	CV	Sensitivity: 0.0428 μA $μM^{-1}$ cm^{-2}	70
			DL: 0.15 nM	
			LDR: 0.5–1800 μM	
ZnO/Yb_2O_3 nanosheets	Hyd	I–V	Sensitivity: 5.063 μA $μM^{-1}$ cm^{-2}	71
			DL: 0.019 ± 0.001 nM	
			LDR: 0.1 nM to 0.1 mM	
$MnCo_xO_y$ nanoparticles	Hyd	I–V	Sensitivity: 0.37 mA μmol L^{-1} cm^{-2}	72
			DL: 0.26 ± 0.01 pmol L^{-1}	
			LDR: 1.0 pmol L^{-1} to 1.0 μmol L^{-1}	
CuO/MnO_2/Gd_2O_3 NSs	3-MPHyd	I–V method	Sensitivity: 24.05 μA $μM^{-1}$ cm^{-2}	This work
			DL: 0.4 ± 0.02 pM (at SNR of 3)	
			LDR: 1.0 pM to 0.1 mM	
			Linearity, $r^2 = 0.9919$	
			Response time: 9.25 s	

Table 1. Performance of hydrazine and their derivatives compounds capturing performances with different nanomaterials by electrochemical method.

the real environmental sample with various concentrations, the fabricated material based on CuO/MnO_2/Gd_2O_3 NSs was used to detect in the industrial effluent (collected from the Jeddah Industrial Area, Saudi Arabia) and extracted samples. The collected industrial effluent was initially filtered to remove the floating large particles and then filtered sample was directly used for analysis. The extracted sample from plastic baby bottle, plastic water bottle, and PVC food packaging bags were also filtered and analysed with CuO/MnO_2/Gd_2O_3 NSs/Nafion/GCE sensor probe by electrochemical method. The analysis report is presented in the Table 2. The results clarified that the proposed NSs has high possibility to selective detection of 3-MPHyd significantly and efficiently.

Conclusions

In this study, selective 3-MPHyd chemical material based on nano-formulated CuO/MnO_2/Gd_2O_3 spike was fabricated and reported in details. The NSs of transition metal oxides were prepared by the hydrothermal approach in alkaline phase at low-temperature. The fabricated nanospikes were totally characterized by using FTIR, UV–Vis,

Real sample	Added 3-MPHyd concentration (μM)	Determined 3-MPHyd concentration by $CuO/MnO_2/Gd_2O_3$ NSs/GCE (μM)	Recovery (%)	RSD (%) (n = 3)
Industrial effluent	0.0100	0.01085	108.5	
	0.0100	0.01033	103.3	5.03
	0.0100	0.009811	98.11	
Plastic baby bottle	0.0100	0.009689	96.89	
	0.0100	0.009407	94.07	1.88
	0.0100	0.009743	97.43	
Plastic water bottle	0.0100	0.01145	114.5	
	0.0100	0.01190	119.0	2.55
	0.0100	0.01202	120.2	
PVC food packaging bag	0.0100	0.01028	102.8	
	0.0100	0.01035	103.5	0.37
	0.0100	0.01029	102.9	

Table 2. Analyses of 3-MPHyd into real environmental sample using $CuO/MnO_2/Gd_2O_3$ NSs/Nafion/GCE sensor probe by electrochemical method.

XRD, XPS and FESEM. The slurry of ternary $CuO/MnO_2/Gd_2O_3$ NSs was coated onto GCE as a layer of thin-film with conducting binder of nafion solution for selective and sensitive electrochemical detection of 3-MPHyd toxic compounds. The important experimental parameters such as sensitivity, low limit of detection, quantification, reaction time, sensitivity and reusability were performed systematically. The obtain results were good and satisfactorily enough to determine the target 3-MPHyd in short response time by electro-chemical approach. Here, $CuO/MnO_2/Gd_2O_3$ NSs materials are an effective and potential for the selective detection of 3-MPHyd. Thus the materials can be used in broad scales for the efficient detection of selective 3-MPHyd by electrochemical method at room conditions for environmental remediation.

Received: 18 April 2019; Accepted: 1 November 2020
Published online: 20 November 2020

References

1. Tiwari, I., Gupta, M., Sinha, P. & Banks, C. E. Simultaneous determination of hydrazine and phenyl hydrazine using 4′-(4-carboxyphenyl)-2,2′:6′,2″ terpyridine diacetonitrile triphenylphosphine ruthenium(II) tetrafluoroborate complex functionalized multiwalled carbon nanotubes modified electrode. *Mater. Res. Bull.* **60**, 166–173 (2014).
2. World Health Organization. *Guidelines for Drinking-Water Quality*. 2nd edn (World Health Organization, Geneva, 1993).
3. US Department of Health. *Human Services* (National Library of Medicine, Bethesda, 1993).
4. NIOSH, Method 3518, *Phenyl hydrazine, Manual of Analytical Methods*, 4th ed., (National Institute for Occupational Safety and Health, Cincinnati 1994).
5. Safavi, A. & Karimi, M. A. Flow injection chemiluminescence determination of hydrazine by oxidation with chlorinated isocyanurates. *Talanta* **58**, 785–792 (2002).
6. Rawat, J. P. & Bhattacharjee, P. Spectrophotometric determination of phenylhydrazine with ammonium molybdate. *Microchim. Acta* **66**, 619–624 (1976).
7. Tangy, W., Jiang, G. & Cai, Z. Determination of atrazine and its deethylated degradation product in water and sediment by using gas chromatography/ion trap mass spectrometry. *Int. J. Environ. Anal. Chem.* **85**, 1117–1125 (2005).
8. Tiwari, I., Gupta, M., Sinha, P. & Aggarwal, S. K. Electro-oxidation of phenyl hydrazine on a modified electrode constructed using nanocomposite of ruthenium terpyridyl complex, multiwalled carbon nanotubes and nafion. *Electrochim. Acta* **76**, 106–111 (2012).
9. Wang, G. *et al.* Copper oxide nanoarray based on the substrate of Cu applied for the chemical sensor of hydrazine detection. *Electrochem. Commun.* **11**, 631–634 (2009).
10. Shukla, S., Chaudhary, S., Umar, A., Chaudhary, G. R. & Mehta, S. K. Tungsten oxide (WO3) nanoparticles as scaffold for the fabrication of hydrazine chemical sensor. *Sens. Actuator B Chem.* **196**, 231–237 (2014).
11. Dai, Y., Huang, J., Zhang, H. & Liu, C. C. Highly sensitive electrochemical analysis of tunnel structured MnO_2 nanoparticle-based sensors on the oxidation of nitrite. *Sens. Actuator B Chem.* **281**, 746–750 (2019).
12. Khan, S. B. *et al.* Highly sensitive and stable phenyl hydrazine chemical sensors based on CuO flower shapes and hollow spheres. *New J. Chem.* **37**, 1098–1104 (2013).
13. Rahman, M. M. *et al.* Fabrication of highly sensitive phenyl hydrazine chemical sensor based on as-grown $ZnO–Fe_2O_3$ microwires. *Int. J. Electrochem. Sci.* **8**, 520–534 (2013).
14. Rahman, M. M., Khan, A., Marwani, H. M. & Asiri, A. M. Hydrazine sensor based on silver nanoparticle-decorated polyaniline tungstophosphate nanocomposite for use in environmental remediation. *Microchim. Acta* **183**, 1787–1796 (2016).
15. Rahman, M. M., Balkhoyor, H. B. & Asiri, A. M. Ultrasensitive and selective hydrazine sensor development based on Sn/ZnO nanoparticles. *RSC Adv.* **6**, 29342–29352 (2016).
16. Sheikh, T. A. *et al.* Trace electrochemical detection of Ni^{2+} ions with bidentate *N*,*N*′-(ethane-1,2-diyl)bis(3,4-dimethoxybenzenesulfonamide) [EDBDMBS] as a chelating agent. *Inorg. Chim. Acta* **464**, 157–166 (2017).
17. Umar, A. *et al.* Enhanced photocatalytic degradation of harmful dye and phenyl hydrazine chemical sensing using ZnO nanourchins. *Chem. Eng. J.* **262**, 588–596 (2015).
18. Ibrahim, A. A. *et al.* Growth and properties of Ag-doped ZnO nanoflowers for highly sensitive phenyl hydrazine chemical sensor application. *Talanta* **93**, 257–263 (2012).
19. Rahman, M. M., Ahmed, J. & Asiri, A. M. Thiourea sensor development based on hydrothermally prepared CMO nanoparticles for environmental safety. *Biosens. Bioelectron.* **99**, 586–592 (2018).
20. Awual, M. R., Hasan, M. M. & Khaleque, M. A. Efficient selenium(IV) detection and removal from water by tailor-made novel conjugate adsorbent. *Sens. Actuators B Chem.* **209**, 194–202 (2015).

21. Awual, M. R. *et al.* Inorganic-organic based novel nano-conjugate material for effective cobalt(II) ions capturing from wastewater. *Chem. Eng. J.* **324**, 130–139 (2017).
22. Awual, M. R. *et al.* Ligand field effect for Dysprosium(III) and Lutetium(III) adsorption and EXAFS coordination with novel composite nanomaterials. *Chem. Eng. J.* **320**, 427–435 (2017).
23. Hussain, M. M., Rahman, M. M., Asiri, A. M. & Awual, M. R. Non-enzymatic simultaneous detection of L-glutamic acid and uric acid using mesoporous Co_3O_4 nanosheets. *RSC Adv.* **6**, 80511–80521 (2016).
24. Xiao, H., Li, P., Jia, F. & Zhang, L. General non-aqueous sol-gel synthesis of nanostructured Sm_2O_3, Gd2O3, Dy_2O_3, and Gd_2O_3:Eu^{3+} phosphor. *J. Phys. Chem. C* **113**, 21034–21041 (2009).
25. Rahman, M. M., Alam, M. M. & Asiri, A. M. Fabrication of an acetone sensor based on facile ternary MnO2/Gd2O3/SnO2 nanosheets for environmental safety. *New J. Chem.* **41**, 9938–9946 (2017).
26. Abdullah, M. M. *et al.* Fabrication of ethanol chemical sensors based on as-prepared Gd_2O_3 nanorods by facile hydrothermal routes. *J. Colloidal Sci. Biotechnol.* **2**, 322–327 (2013).
27. Abdullah, M. M. *et al.* Sensitive and fast response ethanol chemical sensor based on as-grown Gd_2O_3 nanostructures. *J. Rare Earths.* **33**, 214–220 (2015).
28. Rahman, M. M., Hussain, M. M., Asiri, A. M., Alamry, K. A. & Hasnat, M. A. An enzyme free detection of L-Glutamic acid using deposited CuO.GdO nanospikes on a flat glassy carbon electrode. *Surf. Interfaces* **20**, 100617 (2020).
29. Zheng, W. *et al.* Low power high purity red upconversion emission and multiple temperature sensing behaviors in Yb^{3+}, Er^{3+} codoped Gd_2O_3 porous nanorods. *ACS Sustain. Chem. Eng.* **8**, 9578–9588 (2020).
30. Xiao, F. E. N. G., Jun-song, G. A. O. & Zu-cheng, W. U. Removal of copper ions from electroplating rinse water using electrodeionization. *J. Zhejiang Univ. Sci. A.* **9**, 1283–1287 (2008).
31. Rahman, M. M., Alam, M. M., Asiri, A. M. & Islam, M. A. Ethanol sensor development based on ternary-doped metal oxides (CdO/ZnO/Yb_2O_3) nanosheets for environmental safety. *RSC Adv.* **7**, 22627–22639 (2017).
32. Chen, W. *et al.* Peroxidase-like activity of water-soluble cupric oxide nanoparticles and its analytical application for detection of hydrogen peroxide and glucose. *Analyst* **137**, 1706–1712 (2012).
33. Kumar, P. P. N. V., Shameem, U., Kollu, P., Kalyani, R. L. & Pammi, S. V. N. Green synthesis of copper oxide nanoparticles using *Aloe vera* leaf extract and its antibacterial activity against fish bacterial pathogens. *Biol. Nano. Sci.* **5**, 135–139 (2015).
34. Wang, G. S., Nie, L. Z. & Yu, S. H. Tunable wave absorption properties of β-MnO2 nanorods and their application in dielectric composites. *RSC Adv.* **2**, 6216–6221 (2012).
35. Feng, L. *et al.* MnO_2 prepared by hydrothermal method and electrochemical performance as anode for lithium-ion battery. *Nanoscale Res. Lett.* **9**, 290 (2014).
36. Khan, S. A., Gambhir, S. & Ahmad, A. Extracellular biosynthesis of gadolinium oxide (Gd_2O_3) nanoparticles, their biodistribution and bioconjugation with the chemically modified anticancer drug taxol. *Beilstein J. Nanotechnol.* **5**, 249–257 (2014).
37. Jenkins, R. & Snyder, R. L. *Introduction to X-Ray Powder Diffractometry* Vol. 138, 750–950 (Wiley, New York, 1994).
38. Huang, M. *et al.* Merging of Kirkendall growth and Ostwald Ripening: CuO@MnO2 Core-shell architectures for asymmetric supercapacitors. *Sci. Rep.* **4**, 4518–4527 (2014).
39. Padil, V. V. T. & Cerník, M. Green synthesis of copper oxide nanoparticles using gum karaya as a biotemplate and their antibacterial application. *Int. J. Anomed.* **8**, 889–898 (2013).
40. Dubal, D. P., Dhawale, D. S., Salunkhe, R. R., Jamdade, V. S. & Lokhande, C. D. Fabrication of copper oxide multilayer nanosheets for supercapacitor application. *J. Alloys Compd.* **492**, 26–30 (2010).
41. Rahman, M. M., Jamal, A., Khan, S. B. & Faisal, M. CuO co-doped ZnO based nanostructured materials for sensitive chemical sensor applications. *ACS Appl. Mater. Interfaces* **3**, 1346–1351 (2011).
42. Huang, M. *et al.* Merging of Kirkendall Growth and Ostwald Ripening: CuO@MnO_2 core–shell architectures for asymmetric supercapacitors. *Sci. Rep.* **4**, 4518–4526 (2014).
43. Li, L. *et al.* Controlled growth of CuS on electrospun carbon nanofibers as an efficient counter electrode for quantum dot-sensitized solar cells. *J. Phys. Chem. C* **118**, 16526–16535 (2014).
44. Akhavan, O., Azimirad, R., Safa, S. & Hasani, E. CuO/$Cu(OH)_2$ hierarchical nanostructures as bactericidal photocatalysts. *J. Mater. Chem.* **21**, 9634–9640 (2011).
45. Wang, J. G., Yang, Y., Huang, Z. H. & Kang, F. Rational synthesis of MnO_2/conducting polypyrrole@ carbon nanofiber triaxial nano-cables for high-performance supercapacitors. *J. Mater. Chem.* **22**, 16943–16949 (2012).
46. Xia, H. *et al.* Hierarchically structured Co_3O_4@ Pt@ MnO_2 nanowire arrays for high-performance supercapacitors. *Sci. Rep.* **3**, 2978–2985 (2013).
47. Wang, C. *et al.* Controlled synthesis of micro/nanostructured CuO anodes for lithium-ion batteries. *Nano. Energy* **9**, 334–344 (2014).
48. Pawar, S. M. *et al.* Multi-functional reactively-sputtered copper oxide electrodes for supercapacitor and electro-catalyst in direct methanol fuel cell applications. *Sci. Rep.* **6**, 21310–21318 (2016).
49. Patel, S. K. S. *et al.* Structural and magnetic properties of Co-doped Gd_2O_3 nanorods. *J. Magn. Magn. Mater.* **403**, 155–160 (2016).
50. Devi, A. *et al.* Rare-earth substituted HfO_2 thin films grown by metalorganic chemical vapor deposition. *Thin Solid Films* **520**, 4512–4517 (2012).
51. Ren, S. *et al.* Surface modification of sulfonated poly (ether ether ketone) membranes using Nafion solution for direct methanol fuel cells. *J. Membr. Sci.* **247**, 59–63 (2005).
52. Wang, Z., Liu, G., Zhang, L. & Wang, H. Electrochemical detection of trace cadmium in soil using a Nafion/stannum film-modified molecular wire carbon paste electrodes. *Ionics* **19**, 1687–1693 (2013).
53. Rahman, M. M., Alam, M. M. & Alamry, K. A. Sensitive and selective m-Tolylhydrazine sensor development based on CdO nanoparticles decorated multi-walled carbon nanotubes. *J. Ind. Eng. Chem.* **77**, 309–316 (2019).
54. Rahman, M. M., Jamal, A., Khan, S. B., Faisal, M. & Asiri, A. M. Fabrication of phenyl-hydrazine chemical sensor based on Al-doped ZnO nanoparticles. *Sens. Transducers J.* **134**, 32–44 (2011).
55. Akhter, H. *et al.* Fabrication of hydrazine sensor based on silica-coated Fe2O3 magnetic nanoparticles prepared by a rapid microwave irradiation method. *J. Alloys Compd.* **698**, 921–929 (2017).
56. Rahman, M. M., Ahmed, J. & Asiri, A. M. Development of creatine sensor based on antimony-doped tin oxide (ATO) nanoparticles. *Sens. Actuators B Chem.* **242**, 167–175 (2017).
57. Dong, B. *et al.* High dispersion and electrocatalytic activity of Pd/titanium dioxide nanotubes catalysts for hydrazine oxidation. *J. Power Source* **175**, 266–271 (2008).
58. Lu, W., Shu, J., Wang, Z., Haung, N. & Song, W. The intrinsic oxidase-like activity of Ag2O nanoparticles and its application for colorimetric detection of sulfite. *Mater. Lett.* **154**, 33–36 (2015).
59. Yue, X., Yang, W., Xu, M., Liu, X. & Jia, J. High performance of electrocatalytic oxidation and determination of hydrazine based on Pt nanoparticles/TiO_2 nanosheets. *Talanta* **144**, 1296–1300 (2015).
60. Umar, A., Rahman, M. M., Kim, S. H. & Hahn, Y. B. Zinc oxide nanonail based chemical sensor for hydrazine detection. *Chem. Commun. (Camb.)* **2**, 166–168 (2008).
61. Di Zhao, Y., De Zhang, W., Chen, H. & Luo, Q. M. Anodic oxidation of hydrazine at carbon nanotube powder microelectrode and its detection. *Talanta* **58**, 529–534 (2002).

62. Kumar, R. *et al.* Ag-doped ZnO nanoellipsoids: potential scaffold for photocatalytic and sensing applications. *Talanta* **137**, 204–213 (2015).
63. Salimi, A., Miranzadeh, L. & Hallaj, R. Amperometric and voltammetric detection of hydrazine using glassy carbon electrodes modified with carbon nanotubes and catechol derivatives. *Talanta* **75**, 147–156 (2008).
64. Ni, Y., Zhu, J., Zhang, L. & Hong, J. Hierarchical ZnO micro/nanoarchitectures: hydrothermal preparation, characterization and application in the detection of hydrazine. *CrystEngComm* **12**, 2213–2218 (2010).
65. Liu, J., Li, Y., Jiang, J. & Huang, X. C@ ZnO nanorod array-based hydrazine electrochemical sensor with improved sensitivity and stability. *Dalton Trans.* **39**, 8693–8697 (2010).
66. Sultana, W., Ghosh, S. & Eraiah, B. Zinc oxide modified au electrode as sensor for an efficient detection of hydrazine. *Electroanalysis* **24**, 1869–1877 (2012).
67. Han, K. N., Li, C. A., Bui, M. P. N., Pham, X. H. & Seong, G. H. Control of ZnO morphologies on carbon nanotube electrodes and electrocatalytic characteristics toward hydrazine. *Chem. Commun. (Camb).* **47**, 938 (2011).
68. Fang, B., Zhang, C., Zhang, W. & Wang, G. A novel hydrazine electrochemical sensor based on a carbon nanotube-wired ZnO nanoflower-modified electrode. *Electrochim. Acta* **55**, 178–182 (2009).
69. Zhang, C. *et al.* Enhancement in analytical hydrazine based on gold nanoparticles deposited on ZnO-MWCNTs films. *Sens. Actuators B Chem.* **150**, 247–253 (2010).
70. Rahman, M. M., Alam, M. M., Asiri, A. M. & Awual, M. R. Fabrication of 4-aminophenol sensor based on hydrothermally prepared ZnO/Yb_2O_3 nanosheets. *New J. Chem.* **41**, 9159–9169 (2017).
71. Rahman, M. M., Alam, M. M., Asiri, A. M. & Islam, M. A. 3, 4-Diaminotoluene sensor development based on hydrothermally prepared $MnCo_xO_y$ nanoparticles. *Talanta* **176**, 17–25 (2018).
72. Arshad, M. N. *et al.* Fabrication of cadmium ionic sensor based on (E)-4-Methyl-N′-(1-(pyridin-2-yl) ethylidene) benzenesulfonohydrazide (MPEBSH) by electrochemical approach. *J. Organomet. Chem.* **827**, 49–55 (2017).
73. Awual, M. R. *et al.* Facile mercury detection and removal from aqueous media involving ligand impregnated conjugate nanomaterials. *Chem. Eng. J.* **290**, 243–251 (2016).
74. Sheikh, T. A., Rahman, M. M., Asiri, A. M., Marwani, H. M. & Awual, M. R. 4-Hexylresorcinol sensor development based on wet-chemically prepared $Co_3O_4@Er_2O_3$ nanorods: a practical approach. *J. Ind. Eng. Chem.* **66**, 446–455 (2018).
75. Awual, M. R. *et al.* Efficient detection and adsorption of cadmium(II) ions using innovative nano-composite materials. *Chem. Eng. J.* **343**, 118–127 (2018).
76. Rahman, M. M. Selective capturing of phenolic derivative by a binary metal oxide microcubes for its detection. *Sci. Rep.* **9**, 19234 (2019).
77. Rahman, M. M. *et al.* Facile and efficient 3-chlorophenol sensor development based on photolumenescent core-shell CdSe/ZnS quantum dots. *Sci. Rep.* **10**, 557 (2020).
78. Rahman, M. M. & Ahmed, J. Cd-doped Sb_2O_4 nanostructures modified glassy carbon electrode for efficient detection of melamine by electrochemical approach. *Biosens. Bioelectron.* **102**, 631–636 (2018).
79. Rahman, M. M. Efficient formaldehyde sensor development based on Cu-codoped ZnO nanomaterial by an electrochemical approach. *Sens. Actuators B Chem.* **305**, 127541 (2020).
80. Rahman, M. M. Label-free Kanamycin sensor development based on CuONiO hollow-spheres: food samples analyses. *Sens. Actuators: B Chem.* **264**, 84–91 (2018).
81. Rahman, M. M., Wahid, A. & Asiri, A. M. Development of highly sensitive 1, 4-dioxane sensor with semiconductor NiO-doped Nd_2O_3 nanostructures by electrochemical approach. *New J. Chem.* **43**, 17395–17402 (2019).
82. Alam, M. M., Asiri, A. M. & Rahman, M. M. Fabrication of phenylhydrazine sensor with V_2O_5 doped ZnO nanocomposites. *Mater. Chem. Phys.* **243**, 122658 (2020).

Acknowledgements

This project was funded by the National Plan for Science, Technology and Innovation (MAARIFAH)—King Abdulaziz City for Science and Technology—the Kingdom of Saudi Arabia—Award No. (14-BIO1978-03). The authors also, acknowledge with thanks Science and Technology Unit, King Abdulaziz University for technical support.

Author contributions

M.M.R. Designed and performed the experiments and wrote the manuscript text; M.M.A. Performed all sensor applications with fabricated sensor material; A.M.A. Revised the manuscript and provided the technical supports; F.A.D.M.O. Performed the optical characterization of ternary nanostructure materials. Finally, all the authors are revised and approved the manuscript.

Competing interests

The authors declare no competing interests.

Additional information

Correspondence and requests for materials should be addressed to M.M.R.

Reprints and permissions information is available at www.nature.com/reprints.

Publisher's note Springer Nature remains neutral with regard to jurisdictional claims in published maps and institutional affiliations.